Hindawi
International Journal of Antennas and Propagation
Volume 2023, Article ID 1734637, 10 pages
https://doi.org/10.1155/2023/1734637

Research Article

Two-Step Decoupling Design of a Microstrip Antenna Array by Using Waveguided Complementary Split-Ring Resonators and a Fully Connected Neural Network

Wen-Ying Zhou,[1] **Zhong-Lei Mei**,[2] **Mai Lu**,[1] **and Ya-Bo Zhu**[3]

[1]*Key Lab of Opto-Electronic Technology and Intelligent Control of Ministry of Education, Lanzhou Jiaotong University, Lanzhou 730070, China*
[2]*School of Information Science and Engineering, Lanzhou University, Lanzhou 730000, China*
[3]*School of Electronic and Information Engineering, Lanzhou Jiaotong University, Lanzhou 730070, China*

Correspondence should be addressed to Zhong-Lei Mei; meizl@lzu.edu.cn

Received 28 October 2021; Revised 24 July 2022; Accepted 6 April 2023; Published 20 April 2023

Academic Editor: Claudio Curcio

To suppress the mutual coupling between closely-spaced patches, we propose a two-step decoupling design approach for a microstrip antenna array with the dimensions of $44.9 \times 30.495\ \text{mm}^2$. The first step is designing a decoupling unit on the basis of waveguided complementary split-ring resonators (WCSRRs) to improve isolation. The second step is presenting an optimization method by using a fully connected neural network (FCNN) to enhance design efficiency. By inserting WCSRRs structure between two patches with the edge-to-edge distance of $0.24\lambda_0$ (port-to-port distance with $0.66\lambda_0$), where λ_0 is the wavelength of free space at a resonant frequency of 9 GHz, the mutual coupling can be reduced to −29.38 dB, which is confirmed by the EM simulation. We use the simulation results of the array geometries and EM performances to train FCNN at first and then use the trained FCNN to predict the array geometric parameters for the optimal EM response when the edge-to-edge distance between patches is further reduced to $0.21\lambda_0$ and $0.18\lambda_0$ (port-to-port distance reduced to $0.60\lambda_0$ and $0.56\lambda_0$). The measured isolation of the predicted microstrip antenna array is increased to 41.05 dB and 52.33 dB, respectively. Compared to the EM simulation, our FCNN approach has a higher accuracy and lower computational complexity. Therefore, the proposed array predicted by FCNN has a better decoupling performance. All the simulated and predicted results are validated via the measurement to demonstrate the effectiveness of our design scheme. The advantages of our work include the good decoupling performance of the proposed WCSRRs and the convenient optimization of the FCNN from physical response to optimal antenna array geometry design.

1. Introduction

Microstrip antenna arrays can be applied to multiple-input-multiple-output (MIMO) systems, radar applications, modern mobile, and space tracking. Radiating patches of the antenna array are not isolated, and they are mutually coupled with each other. For the array's elements, the mutual coupling may adversely affect the input impedance, gain, sidelobe level, and radiation pattern [1]. Moreover, the decoupling design methods of the antenna are generally solved by the empirical formula and full electromagnetic (EM) simulation. These two traditional design methods are inherently limited. The calculated antenna results by empirical formulas are affected by relative permittivity and tangent loss of the dielectric substrate, while the optimization process of EM simulation is time-consuming and the computational cost increases drastically with increasing structure complexity. The multiparameter optimization can easily result in millions of calculations.

From the aspect of decoupling unit design, there are many methods to decrease the mutual coupling such as using a defected ground structure (DGS) [2, 3], an electromagnetic band-gap (EBG) structure [4], a frequency selective surface (FSS) superstrate [5], or adopting the hybrid

wideband structure [6]. Besides, a cascaded and a dual-band decoupling network (DN) were proposed for antenna decoupling [7–9], and incorporating a waveguide metamaterial (WG-MTM) structure could also help in obtaining a good decoupling performance [10]. However, the partial power of the source antenna would be radiated from the slot of the DGS structure, which could cause a strong backward radiation pattern. The processing of EBG structures is rather complicated, some of which require an intermediate layer or metal via a hole, and the elements of other structures are too complex in the references. Many MTM units have a good decoupling performance with a simple and compact structure.

From the aspect of the optimization methods, different artificial intelligence techniques have been used in modern antenna design to overcome the computational cost problem of numerical optimization. Artificial intelligent algorithms can find correlations between input and output variables much efficiently and can thus speed up the optimization process. It has been used in the design of metamaterial perfect absorbers [11], and estimation of the radiation performance of antenna arrays [12]. In [13], machine learning (ML) was used to design a nanomagnetic-based antenna by mapping the particle radius. Aguni et al. [14] used artificial neural networks (ANN) to design a dual-band microstrip patch antenna fed by a coplanar waveguide, and Sharma et al. [15] designed a double T-shaped antenna and optimized it by using selection operator, ANN, and k-nearest neighbor methods, and Khan and Roy [16] predicted the slot-position and slot-size of a microstrip antenna by using support vector regression. The multiperformance optimization of an antenna array was estimated by a multibranch ANN model and a multistage collaborative ML algorithm, respectively [17, 18]. Recently, the deep neural network (DNN) was used to design nanostructure for phase manipulation [19, 20], and inversely designed the broadband quasi-Yagi antenna [21]. ML has been applied in antenna design as a good calculation tool.

In this article, we propose a two-step decoupling design of the microstrip antenna array. The first step is to design the decoupling unit WCSRRs on the basis of waveguide and complementary split ring resonators (CSRR), and propose the microstrip antenna array with WCSRRs by EM simulation; the second step is to optimize and predict the geometry parameters of the proposed array by FCNN. Different from the existing waveguided decoupling studies [22], the proposed WCSRRs cover the central substrate of the array directly to suppress the mutual coupling and improve the isolation of the microstrip antenna array. To optimize the proposed array with WCSRRs when the distance between patches is further reduced, we use FCNN to learn the relationship between array geometry and EM response, and to predict the optimal geometry of the proposed array for on-demand isolation requirement. On the basis of the computability of large-volume prediction data, the decoupling performance of the arrays predicted by FCNN is better than the array designed by EM simulation.

2. Methods and Design

2.1. Proposed Microstrip Antenna Array with WCSRR Design

2.1.1. Geometry of the Proposed Microstrip Antenna Array. According to the microstrip antenna design principle [23], the input impedance [24], and the radiation conductance calculated method [25], the reference microstrip antenna array is proposed. The layout of its structure is shown in Figure 1(a).

The material of Teflon with a permittivity of 2.65 and a thickness of 1 mm is selected as the substrate. The proposed reference antenna array operates at 9 GHz, and its optimal dimensions by EM simulation are as follows: $a = 9.34$ mm, $b = 12.3$ mm, $c = 5.76$ mm, $d_1 = 5.76$ mm, $w_1 = 0.59$ mm, $w_2 = 2.63$ mm, and $e = 9.635$ mm. The distance L between the two patches is $0.24\lambda_0$ (8 mm), where λ_0 is the wavelength of the free space at 9 GHz. To suppress the mutual coupling of the reference antenna array, the decoupling units of WCSRRs are proposed, and its compositional structure is shown in Figure 1(b). The proposed antenna array with WCSRRs in Figure 1(c) is obtained by loading a 1×5 array of WCSRRs on the center of the reference microstrip antenna array, and its backside is covered with the copper layer as shown in Figure 1(d). Every WCSRR unit cell consists of the CSRR and the waveguide on both sides of it, and its structure is shown in Figure 2. As the decoupling unit between the patches, the five CSRR units are directly printed on the substrate, and the waveguide is covered on the CSRRs. It is easy to achieve, and the complexity of our proposed approach is low. When the electric field of the electromagnetic wave is perpendicular to the CSRR plane, an electric resonance will be excited, resulting in an effect such as the electromagnetic band gap.

2.1.2. WCSRR Unit Cell Design. The 3D view of the WCSRR unit cell and its dimensions are shown in Figure 2(a). The proposed WCSRR structure combines waveguide (WG) with complementary split ring resonators (CSRR), which is a kind of waveguided metamaterial (WG-MTM) structure. The waveguide consists of one Teflon layer and two copper layers. As a simple classic structure of the single negative metamaterials, the CSRR has the characteristic of negative permittivity. When the electromagnetic wave resonates with the CSRR unit, the electromagnetic wave would be stopped from propagating. To avoid the unnecessary backward radiation caused by grooving the ground, the CSRR is inserted in the middle of the waveguide structure. The CSRR layer is made of copper, which is sandwiched between two Teflon layers with a thickness of 1 mm. Both the top and bottom Teflon layers are covered with two copper layers, with a thickness of 0.035 mm. The geometric parameters of CSRR, optimized by CST Microwave Studio are as follows: $P = 5$ mm, $D = 3.6$ mm, $w = 0.4$ mm, $g = 0.4$ mm, and $h = 1$ mm, as shown in Figure 2(b).

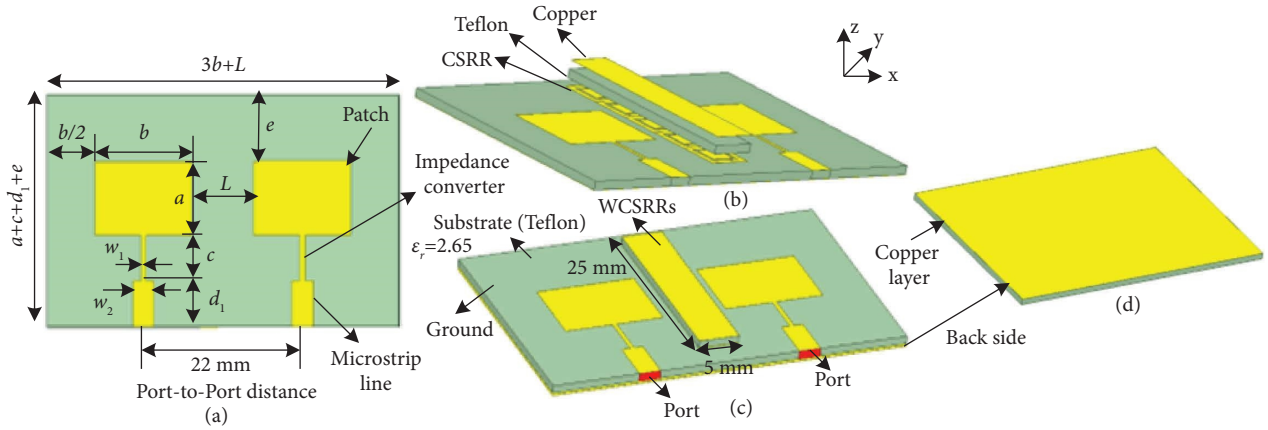

Figure 1: Schematic of the proposed microstrip antenna array. (a) Layout of the reference microstrip antenna array. (b) Compositional structure. (c) Proposed antenna array with WCSRRs. (d) Backside of the proposed antenna array.

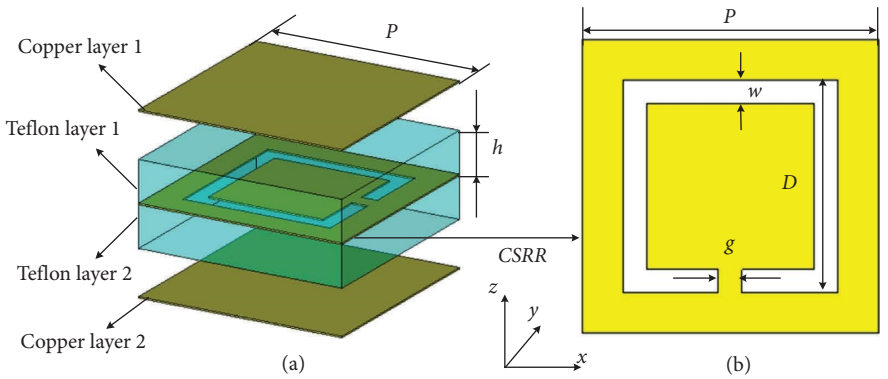

Figure 2: Structure of the decoupling unit. (a) WCSRR unit cell compositional structure. (b) CSRR unit.

Assuming that a z-polarized electromagnetic wave impinges on the surface of the CSRR along the direction of the $+y$ axis (please refer to Figure 2(a)), then the scattering parameters of the CSRR at 9 GHz can be calculated, and the simulated results are shown in Figure 3(a). The calculated real parts of the effective permittivity and permeability are shown in Figure 3(b).

As shown in Figure 3(a), the electromagnetic wave cannot pass through the CSRR at 9 GHz. The real part of the effective permittivity is negative, and the real part of the effective permeability is positive, as shown in Figure 3(b). These results indicate that the CSRR unit cell is a single negative permittivity material, and can be used to obtain decoupling performance. The decoupling structure of the waveguide cavity is covered with a copper layer, which prevents the incident electromagnetic waves from radiating outward.

The geometry of the patch and CSRR is separately optimized to obtain a high accuracy, and the process of decomposing the whole structure into several parts for optimization separately is a local optimization process. The proposed microstrip antenna array with WCSRRs in Figure 1 is based on the locally optimal parameters of the EM simulation. To optimize all the geometric parameters of individual patches and CSRRs at the same time is a global optimization process. The reason for our global optimization approach is that while using local optimization it can improve the solution efficiency, but the optimal decoupling performance of the whole proposed array becomes difficult to obtain. To overcome this issue, we use FCNN to achieve global optimization more efficiently.

2.2. FCNN Approach. FCNN is a type of artificial neural network where the architecture is such that all the neurons in one layer are connected to the neurons in the next layer [26]. The information is interconnected through a group of artificial neutrons, where each node produces a nonlinear function of its input. Its complex relationship could be effectively learned by multilayer perceptrons (MLPs) [27]. Our FCNN scheme is established under the TensorFlow framework as shown in Figure 4. Its MLPs consist of an input layer, variable hidden layers, and an output layer, and every hidden layer has variable artificial neutrons. In order to achieve fast convergence, the MLPs are trained by the adaptive moment estimation (Adam) algorithm. On the basis of the adaptive estimates of lower-order moments, the Adam algorithm adapts to the first-order gradient-based

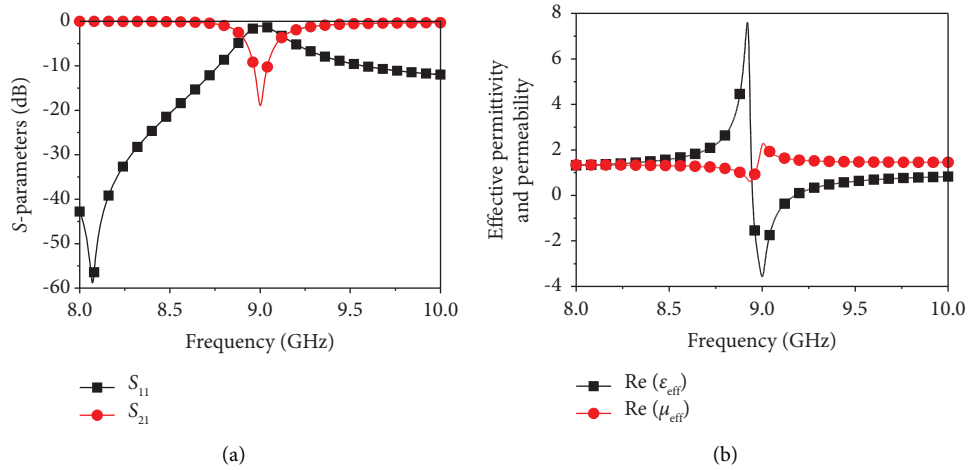

Figure 3: Simulated results of the CSRR. (a) S parameters. (b) Retrieved effective permittivity and permeability.

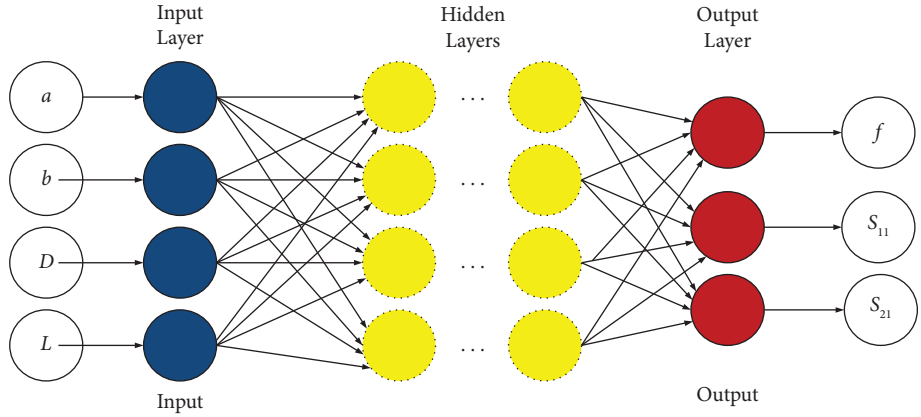

Figure 4: FCNN scheme.

optimization of the stochastic objective functions. The output corresponding to the input is computed by the forward propagation formula as follows:

$$y_j = A\left(\sum_i w_{i,j}x_i\right) + b_j, \tag{1}$$

where y_j (the features of training: the S-parameters response of the proposed array) is the output signal, x_i (the geometric parameters of the proposed array) is the input signal, A is the activation function, and the rectified linear unit (ReLU) is used as the activation function to avoid the gradient explosion or disappearance. Both the weights $w_{i,j}$ and the bias value b_j are generated by random initialization, and they are further updated by the Adam algorithm.

Through the forward training by FCNN in Figure 4, the relationship between geometric parameters and S-parameters response is obtained. In the following part, we will utilize it to predict the geometric parameters of the proposed array for obtaining the optimal decoupling, when the distance of patches is further reduced.

3. Results and Discussion

3.1. Results by EM Simulation. By using EM simulation, we simulate the parameters and the radiation patterns of both the reference array and the proposed array, respectively. The local optimization scheme is as follows: the geometric parameters a and b of the patch are first optimized to design the reference array, and then the geometric parameter D of CSRR is parametrically optimized to give an isolated array with WCSRRs. As Figure 5(a) shows, both arrays are resonant at 9 GHz and their reflection coefficients (S_{11}) are less than −25 dB. The mutual coupling (S_{21}) of the proposed antenna array with WCSRR is improved by nearly 8 dB compared with that of the reference antenna at a resonant frequency. The simulated results are shown in Figure 5(a). A good agreement of the radiation pattern is obtained between the proposed antenna arrays with WCSRRs and the reference array, and the gain varies from 7.6 dBi to 7.4 dBi after adding the decoupling element in the reference microstrip array, as shown in Figure 5(b). It reveals that the proposed antenna array with WCSRRs could reduce the mutual coupling effectively without affecting the reflection coefficient and the radiation pattern.

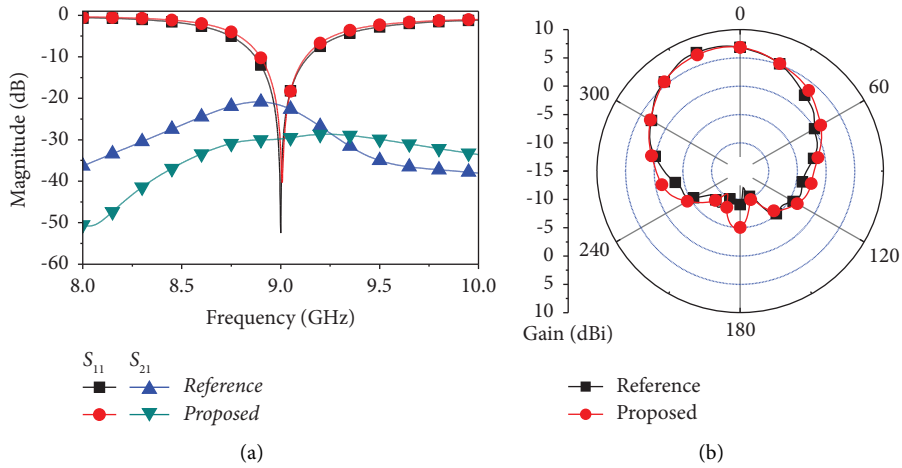

Figure 5: Simulated scattering parameters. (a) S_{11} and S_{21}. (b) Radiation patterns.

Figure 6 shows the simulated surface current distribution of two arrays. When the left patch is excited, the induced current density on the right unexcited patch is significantly reduced after loading the proposed WCSRRs structure. It shows that the WCSRRs structure can suppress the mutual coupling between the patches.

To obtain the optimal decoupling performance of the array with reduced distance between patches, the calculation accuracy must be further increased simultaneously, which means a higher computation in our simulation. Due to the limited computing ability of EM simulation, we introduce FCNN to solve the computationally high precision optimization problems, which aims to predict the geometrical parameters for the optimal EM response.

3.2. Predicted Result by FCNN. Without considering the influence of dielectric substrate, there are four critical geometric parameters which have a major impact on the performance of the proposed antenna array with WCSRRs. They are a, b, D, and L. Therefore, the geometric parameters of the proposed array with WCSRRs need to be optimized in the following range: $a \in [8.5\text{mm}, 10\text{mm}]$, $b \in [8\text{mm}, 14\text{mm}]$, $D \in [0.5\text{mm}, 5\text{mm}]$, and $L \in [6\text{mm}, 8\text{mm}]$. The low-fidelity accuracy means that the optimization step length of a, b, and D is 0.5 mm, and it is 1 mm for L. The complete S-parameters are composed of 2001 frequency points uniformly distributed among the frequency range of 8~10 GHz with an interval of 0.001 GHz. It needs 64 hours to optimize all 1560 data generated from the global optimization calculation in the EM simulation (the configuration of PC: Intel i7 CPU, 64 G RAM, GPU with 4 GB VRAM, and 2 TB Hard Drive). The high-fidelity accuracy is essential to meet the needs of the accurate model design. It means that the optimization step of b and D reduces to be 0.1 mm, a reduces to be 0.01 mm, and it is still 1 mm for L, which would lead to more than 1.2 million possible configurations. EM simulation will need months to compute such an enormous amount of data, and it is hard to search the satisfactory geometric parameters of the proposed array according to its S-parameters performance. For breaking the calculated limitations of EM simulation and shortening the global optimization time, a FCNN is used to predict the high-fidelity geometric parameters of the proposed array when L is reduced from 8 mm to 7 mm and 6 mm, respectively.

By using the 1560 simulated data obtained by EM simulation (low-fidelity geometric parameters data of global optimization), we trained two different FCNN networks for S_{11} and S_{21} responses, respectively. The training network of the geometric parameters versus S_{11} contains 3 hidden layers with 500 neurons per layer, and it took only 4 minutes to complete the 1400 iterations. The training network of the geometric parameters versus S_{21} contains 12 hidden layers with 1300 neutrons per layer, and it took 58 minutes to complete the 2000 iterations. According to the low-fidelity data training results, the 1.27 million high-fidelity geometric parameters data of the proposed array are predicted only in 2 minutes. In the frequency range of 8~10 GHz, the 100 test groups of geometric parameters are chosen randomly from the prediction array. The predicted and simulated results of the proposed array performance in 100 test groups are shown in Figure 7, the reflection ($|S_{11}|$) comparison is shown in Figure 7(a), and the isolation ($|S_{21}|$) comparison is shown in Figure 7(b).

Figure 7 shows that the prediction results and simulation results have consistent variation trends; however, the specific peak values have differences. In general, the reflection and isolation of the predicted values are better. It indicates that excellent predictions could be obtained by the proposed FCNN approach.

On the basis of the optimal prediction geometry of the proposed array corresponding to the best S-parameter response, three new geometric of microstrip antenna arrays are obtained, where L is 8 mm, 7 mm, and 6 mm, respectively (the specific geometric parameters are shown in Table 1). We use EM simulation to simulate their structures to get the S-parameters and radiation patterns for comparison.

Figure 8 shows the comparison of both results. The resonant frequency of the predicted antenna arrays is nearly at 9 GHz, and both reflection and isolation can meet the actual application requirements. After adding athe

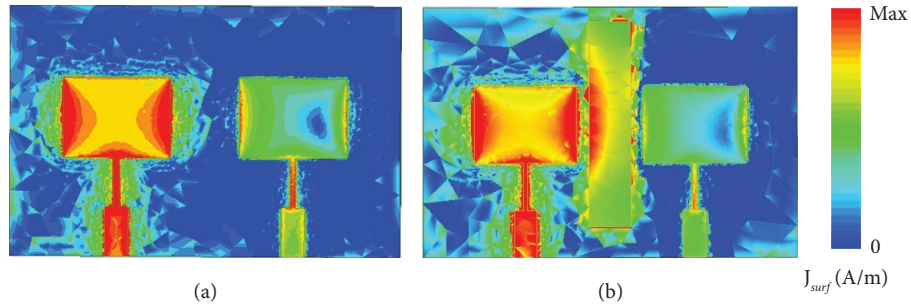

Figure 6: Surface current distribution. (a) Reference antenna array. (b) Antenna array with WCSRR.

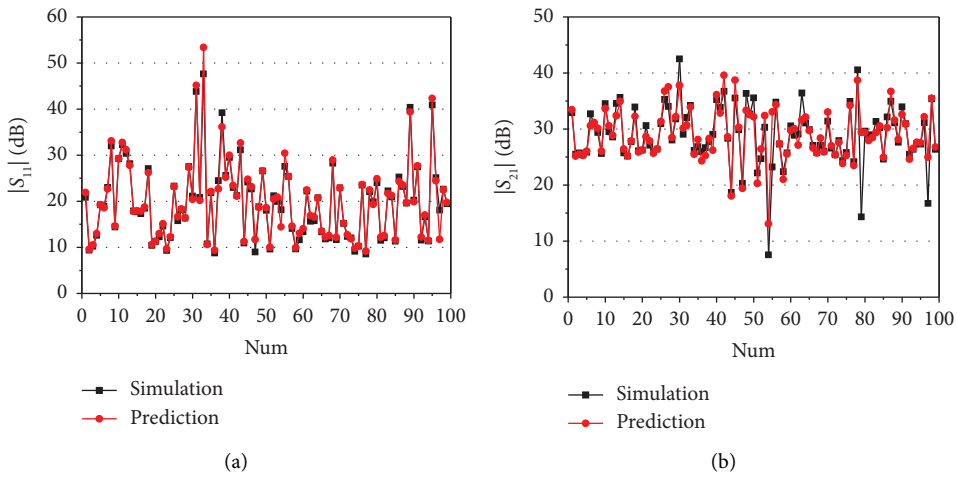

Figure 7: Comparison of predicted and simulated S-parameters response. (a) Reflection $|S_{11}|$. (b) Isolation $|S_{21}|$.

Table 1: Comparison of simulated and measured results of the proposed arrays by different design methods.

Design	Geometric parameters (mm)				S_{21} (dB)		S_{11} (dB)	
					Simulated	Measured	Simulated	Measured
FCNN	$L = 8$	$a = 9.23$	$b = 14.0$	$D = 2.3$	−38.24	−39.09	−17.89	−29.11
	$L = 7$	$a = 9.32$	$b = 13.0$	$D = 2.5$	−40.45	−41.05	−28.02	−37.34
	$L = 6$	$a = 9.42$	$b = 12.6$	$D = 2.5$	−62.20	−52.33	−33.12	−30.60
EM	$L = 8$	$a = 9.34$	$b = 12.3$	$D = 3.6$	−29.48	−31.32	−30.68	−26.81

decoupling element, when $L = 8$ mm, the isolation is increased from 25.53 dB to 38.24 dB, and the gain varies from 7.7 dBi to 7.5 dBi. When $L = 7$ mm, the isolation is increased from 23.33 dB to 40.45 dB, and the gain varies from 7.5 dBi to 7.1 dBi. When $L = 6$ mm, the isolation is increased from 22.66 dB to 62.20 dB, and the gain varies from 7.4 dBi to 7 dBi. It reveals that the decoupling performance of the proposed array is improved obviously, and its radiation performance has little been affected.

The radiation efficiency of the predicted antenna array is simulated, and the results are shown in Figure 9. It reveals that in the operating frequency band (<−10 dB) from 8.95 to 9.15 GHz, the radiation efficiency of the predicted antenna array varies from 98.51%~92.32% when $L = 8$ mm, the radiation efficiency of the predicted antenna array varies from 99.6%~86.46% when $L = 7$ mm, and the radiation efficiency of the predicted antenna array varies from 99.77%~80.13% when $L = 6$ mm. All the maximum values are at 9 GHz.

3.3. Measurement Comparison between the EM Simulated Design and FCNN Design. To further prove the advantage of FCNN compared to the EM simulation, the proposed antenna array designed by EM simulation was fabricated, and its prototype is shown in Figure 10(a). Three newly predicted arrays designed by FCNN were also fabricated, and their prototypes are shown in Figures 10(b)~10(d).

The prototypes of the abovementioned proposed arrays were measured, and the results are shown in Figure 11. Figure 11 shows that, the experimental results are consistent with the simulation results and the operating frequency is nearly 9 GHz. As the distance between patches is further reduced, the requirements for machining accuracy have also

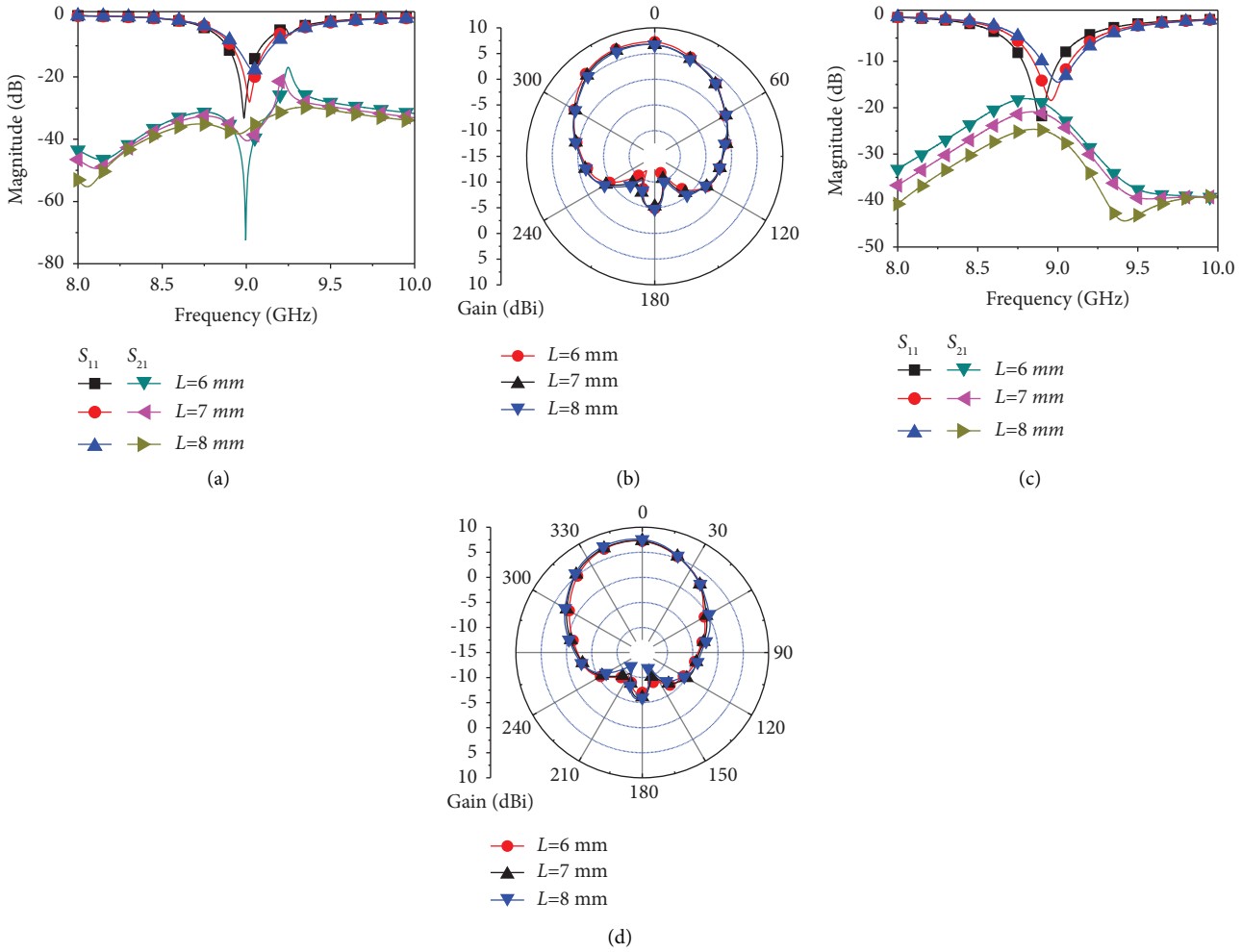

FIGURE 8: Comparison results of the predicted microstrip antenna arrays. (a) S parameters (with WCSRRs). (b) Radiation patterns (with WCSRRs). (c) S parameters (without WCSRRs). (d) Radiation patterns (without WCSRRs).

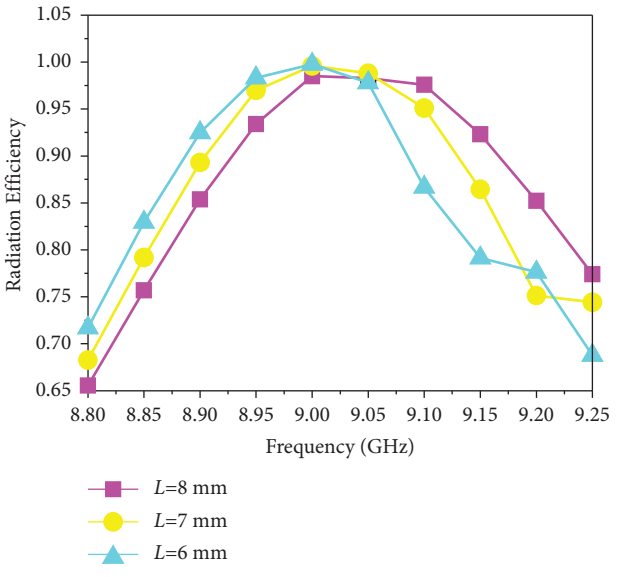

FIGURE 9: Radiation efficiency comparison of the predicted antenna arrays.

increased, which lead to fluctuations in the S_{21} curves and discrepancies between the two cases. It is worth noting that the measurement values of S_{21} are lower than their simulation values basically, and the differences between measurement values and simulation values are acceptable in practical applications. From Figure 11(c), it can be known that the measurement results of the radiation pattern are basically consistent with the simulation results. The comparison results indicate that the decoupling element will not affect the radiation pattern of the predicted arrays. At the operating frequency, there is a detailed S-parameter performance comparison of the proposed arrays designed by FCNN and EM simulation in Table 1.

As shown in Table 1, when $L = 8$ mm, FCNN can improve the isolation of the proposed array by 29.7% compared to EM simulation. Besides that, the measured S_{21} of all the predicted arrays are all less than −39.09 dB basically, revealing a good decoupling performance, and that of the measured S_{11} are all less than −29.11 dB, thus meeting engineering requirements. Especially, when $L = 6$ mm, the measured S_{21} is improved to −52.33 dB. The results

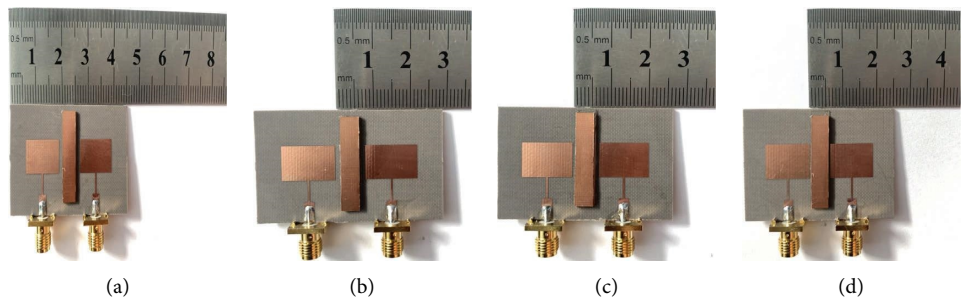

FIGURE 10: Photographs of the proposed array fabrication (unit: mm). (a) Proposed array design by EM simulation. (b) Proposed array predicted by FCNN ($L = 8$). (c) Proposed array predicted by FCNN ($L = 7$). (d) Proposed array predicted by FCNN ($L = 6$).

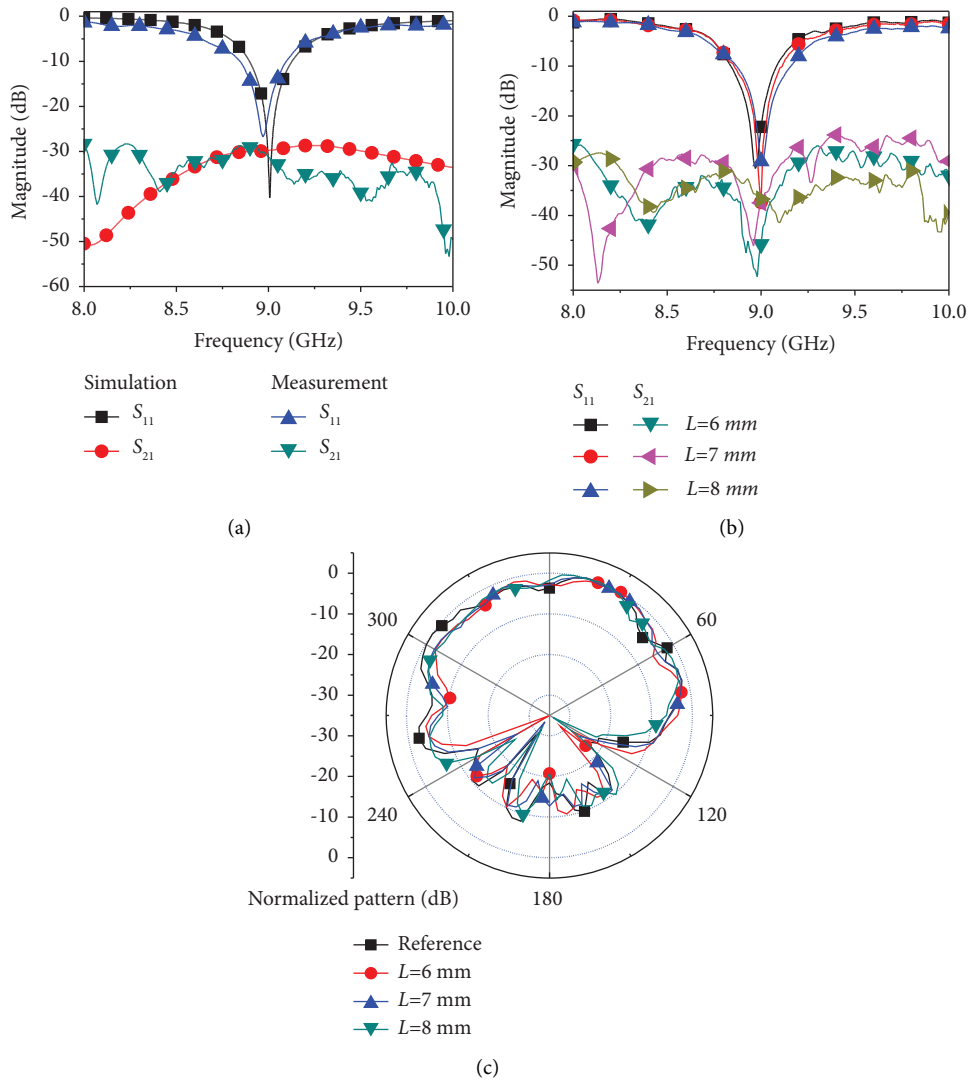

FIGURE 11: Measurement results of the proposed arrays. (a) S parameters comparison results of the array design by EM simulation. (b) S parameters comparison measurement results of predicted arrays design by FCNN. (c) Normalized radiation pattern comparison results of the reference array and predicted array.

demonstrate that the benefits of using FCNN in our design are multifaceted, and it not only provides a higher accuracy of isolation, but also requires less computational power, and has a faster calculation.

The proposed WCSRRs is compared with the previous representative decoupling structure, i.e., DGS, EBG, FSS, DN, and WG-MTM, and the results are listed in Table 2. Different from the design method of other references, the

Table 2: Comparison of the proposed antenna array with previous decoupling works.

References	Decoupling approach/profile (mm^2)	Edge-to-edge distance (mm)	Max. Isolation improvement (dB)	Design complexity	Radiation pattern deterioration
[2]	DGS/128.2 × 14.6	$0.2\lambda_0$	30	Low	No
[3]	DGS/130 × 130	$0.19\lambda_0$	15	Moderate	No
[4]	EBG/55 × 28	$0.11\lambda_0$	18	High	Yes
[5]	FSS/20 × 16	$0.5\lambda_0$	10	Moderate	—
[9]	DN/80 × 60	$0.056\lambda_0$	24	Moderate	Yes
[10]	WG-MTM/76.4 × 91	$0.125\lambda_0$	20	Moderate	No
[22]	WG-MTM/35 × 69.5	$0.11\lambda_0$	10	Moderate	No
Prop.	WCSRRs/(in Figure 1)	$0.24\lambda_0/0.21\lambda_0/0.18\lambda_0$	30	Low	No

antenna arrays with WCSRRs are predicted by FCNN. The comparison results reveal that the geometric dimensions of the predicted antennas are relatively small and have a good isolation. Besides that, the proposed decoupling microstrip antenna array has a low design complexity and no radiation pattern deterioration.

4. Conclusion

For the implementation of the decoupling design of the microstrip antenna array, a two-step approach is proposed to solve the two key factors, (1) the decoupling unit design and (2) the high-fidelity geometric parameters global optimization. First, we design a novel WCSRR structure to reduce the mutual coupling between the closely spaced patches in an H-plane array. By suppressing the surface waves through the proposed structure, the mutual coupling is further decreased by 8 dB compared with the reference antenna array. The proposed WCSRR structure has no adverse impact on the radiation pattern. Second, a global optimization design scheme by using FCNN is used to predict the accurate geometric parameters of the proposed array when the distance between patches is further reduced. It needs 64 hours to obtain the low-fidelity training data obtained by EM simulation, and the high-fidelity geometric parameters can be predicted only in 62 minutes by the FCNN, which cannot be obtained by the EM simulation. The simulated isolation of the predicted arrays increases from 38.24 dB to 62.20 dB as the patch distance decreases from 8 mm to 6 mm, the corresponding gain decreases from 7.5 dBi to 7 dBi, and the radiation efficiency increases from 98.15% to 99.77%. The simulated results have been confirmed by the measurement of their prototype. Compared with the EM simulation, FCNN has a greater computational ability to improve the design efficiency of complex antennas significantly. The proposed decoupling design approach has the potential to be applied in the MIMO antenna and RADAR array designs.

Data Availability

The data used to support the findings of this study are available from the corresponding author upon request.

Conflicts of Interest

The authors declare that they have no conflicts of interest.

Acknowledgments

This study was supported by the National Natural Science Foundation of China (Grant nos. 62161017, 61701208, and 61631007), the Natural Science Foundation of Gansu Province (Grant nos. 21JR7RA283 and 20JR10RA604), and the Tianyou Youth Talent Lift Program of Lanzhou Jiaotong University (Grant no. 1520260111).

References

[1] K. V. Babu and B. Anuradha, "Design of UWB MIMO antenna to reduce the mutual coupling using defected ground structure," *Wireless Personal Communications*, vol. 118, no. 4, pp. 3469–3484, 2021.

[2] S. Biswas, C. K. Ghosh, S. Banerjee, S. Mandal, and D. Mandal, "High port isolation of a dual polarized microstrip antenna array using DGS," *Journal of Electromagnetic Waves and Applications*, vol. 34, no. 6, pp. 683–696, 2020.

[3] C. Zhao, X. P. Li, C. Sun, and H. Huang, "Reduction of mutual coupling between patch antennas using defected ground structure in Land S-bands," *Microwave and Optical Technology Letters*, vol. 61, no. 12, pp. 2730–2738, 2019.

[4] A. K. Biswas and U. Chakraborty, "Reduced mutual coupling of compact MIMO antenna designed for WLAN and WiMAX applications," *International Journal of RF and Microwave Computer-Aided Engineering*, vol. 29, no. 3, Article ID 21629, 2019.

[5] M. Akbari, M. M. Ali, M. Farahani, A. Sebak, and T. Denidni, "Spatially mutual coupling reduction between CP-MIMO antennas using FSS superstrate," *Electronics Letters*, vol. 53, no. 8, pp. 516–518, 2017.

[6] X. J. Zou, G. M. Wang, Y. W. Wang, and B. F. Zong, "Mutual coupling reduction of quasi-Yagi antenna array with hybrid wideband decoupling structure," *AEU-International Journal of Electronics and Communications*, vol. 129, Article ID 153553, 2021.

[7] M. Li, Y. Zhang, D. Wu, K. L. Yeung, L. Jiang, and R. Murch, "Decoupling and matching network for dual-band MIMO antennas," *IEEE Transactions on Antennas and Propagation*, vol. 70, no. 3, pp. 1764–1775, 2022.

[8] M. Li, M. Wang, L. Jiang, and L. K. Yeung, "Decoupling of antennas with adjacent frequency bands using cascaded decoupling Network," *IEEE Transactions on Antennas and Propagation*, vol. 69, no. 2, pp. 1173–1178, 2021.

[9] X. J. Zou, G. M. Wang, Y. W. Wang, and H. P. Li, "An efficient decoupling network between feeding points for multielement linear arrays," *IEEE Transactions on Antennas and Propagation*, vol. 67, no. 5, pp. 3101–3108, 2019.

[10] X. M. Yang, X. G. Liu, Y. Z. Xiao, and J. C. Tie, "Reduction of mutual coupling between closely packed patch antennas using waveguided metamaterials," *IEEE Antennas and Wireless Propagation Letters*, vol. 11, pp. 389–391, 2012.

[11] C. Han, B. Zhang, H. Wang, and J. Ding, "Metamaterial perfect absorber with morphology-engineered meta-atoms using deep learning," *Optics Express*, vol. 29, no. 13, pp. 19955–19963, 2021.

[12] A. M. Ahmed, U. S. K. Thanthrige, A. E. Gamal, and A. Sezgin, "Deep learning for DOA estimation in MIMO radar systems via emulation of large antenna arrays," *IEEE Communications Letters*, vol. 25, no. 5, pp. 1559–1563, 2021.

[13] C. Gianfagna, H. Yu, M. Swaminathan, R. Pulugurtha, R. Tummala, and G. Antonini, "Machine-learning approach for design of nanomagnetic-based antennas," *Journal of Electronic Materials*, vol. 46, no. 8, pp. 4963–4975, 2017.

[14] L. Aguni, A. El Yassini, S. Chabaa, S. Ibnyaich, and A. Zeroual, "Design of a symmetric CPW-fed patch Antenna for WLAN/WIMAX applications Using ANN," *Wireless Personal Communications*, vol. 115, no. 1, pp. 439–456, 2020.

[15] Y. Sharma, H. H. Zhang, and H. Xin, "Machine learning techniques for optimizing design of double T-shaped monopole antenna," *IEEE Transactions on Antennas and Propagation*, vol. 68, no. 7, pp. 5658–5663, 2020.

[16] T. Khan and C. Roy, "Prediction of slot-position and slot-size of a microstrip antenna using support vector regression," *International Journal of RF and Microwave Computer-Aided Engineering*, vol. 29, no. 3, Article ID 21623, 2019.

[17] L. Yuan, X. S. Yang, C. Wang, and B. Z. Wang, "Multibranch artificial neural network modeling for inverse estimation of antenna array directivity," *IEEE Transactions on Antennas and Propagation*, vol. 68, no. 6, pp. 4417–4427, 2020.

[18] Q. Wu, H. Wang, and W. Hong, "Multistage collaborative machine learning and its application to antenna modeling and optimization," *IEEE Transactions on Antennas and Propagation*, vol. 68, no. 5, pp. 3397–3409, 2020.

[19] L. Jiang, X. Z. Li, Q. X. Wu, L. Wang, and L. Gao, "Neural network enabled metasurface design for phase manipulation," *Optics Express*, vol. 29, no. 2, pp. 2521–2528, 2021.

[20] Y. Li, Y. J. Xu, M. L. Jiang et al., "Self-Learning perfect optical chirality via a deep neural network," *Physical Review Letters*, vol. 123, no. 21, Article ID 213902, 2019.

[21] W. Y. Zhou, Z. L. Mei, M. Lu, and Y. B. Zhu, "Deep learning for inverse design of broadband quasi-Yagi antenna," *International Journal of RF and Microwave Computer-Aided Engineering*, vol. 2023, Article ID 7819156, 12 pages, 2023.

[22] C. Z. Guo, H. Q. Zhai, and S. B. Liu, "A new dual-band microstrip antenna array with high isolation by waveguided metamaterial structure," *Microwave and Optical Technology Letters*, vol. 61, no. 5, pp. 1365–1370, 2019.

[23] J. Q. Howell, "Microstrip Antennas," *IEEE Transactions on Antennas and Propagation*, vol. 23, no. 1, pp. 90–93, 1975.

[24] M. D. Deshpande and M. C. Bailey, "Input impedance of microstrip antennas," *IEEE Transactions on Antennas and Propagation*, vol. 30, no. 4, pp. 645–650, 1982.

[25] H. Sobal, "Radiation conductance of open-circuit microstrip (correspondence)," *IEEE Transactions on Microwave Theory and Techniques*, vol. 19, no. 11, pp. 885–887, 1971.

[26] K. Kobayashi, A. Bolatkan, S. Shiina, and R. Hamamoto, "Fully-connected neural networks with reduced parameterization for predicting histological types of lung cancer from somatic mutations," *Biomolecules*, vol. 10, no. 9, p. 1249, 2020.

[27] T. Kim and T. Adali, "Approximation by fully complex multilayer perceptrons," *Neural Computation*, vol. 15, no. 7, pp. 1641–1666, 2003.